

Inhomogeneous magnetism in decagonal $\text{Al}_{69.8}\text{Pd}_{12.1}\text{Mn}_{18.1}$

D. Rau,* J. L. Gavilano, Sh. Mushkolaj, C. Beeli, M. A. Chernikov, and H. R. Ott

Laboratorium für Festkörperphysik, ETH Zürich, 8093 Zürich, Switzerland

(Dated: November 18, 2018)

Abstract

We report the results of measurements of ^{27}Al and ^{55}Mn NMR spectra, the related spin-lattice relaxation rates, and the dc magnetic susceptibility of the stable decagonal quasicrystal $\text{Al}_{69.8}\text{Pd}_{12.1}\text{Mn}_{18.2}$. The temperature-variation of the magnetic susceptibility $\chi(T)$ reveals that the Mn ions carry only an average magnetic moment of approximately $2\mu_B$, and confirms a spin-glass type freezing of the Mn-moments at $T_f = 12\text{K}$. The NMR spectra reveal two partially resolved lines for the ^{27}Al -nuclei, indicating that there are two different sets of environments for the Al-sites. The integrated intensity of the Mn line in the spectra suggests that about half of the Mn ions carry no magnetic moment. Below 50K, and upon decreasing the temperature, the ^{27}Al NMR-linewidth w and the spin-lattice relaxation rate T_1^{-1} both grow with an increasingly negative slope, as it is often observed and interpreted as a critical "slowing down" of magnetic moments in systems approaching a spin-glass transition. Various features, such as a broad maximum in $T_1^{-1}(T)$ and a slope change in the $w(\chi)$ plot, both around 120K, suggest a gradual reduction of the number of Mn moments with decreasing temperature below 120K.

PACS numbers: 61.44.Br., 76.60.-k, 75.50.Lk

*Electronic address: drau@solid.phys.ethz.ch

A. Introduction

Since the discovery of quasicrystalline systems by Shechtman et al. in 1982[1], substantial progress in the understanding of quasicrystalline structures has been made[2, 3, 4]. Quasicrystalline structures are characterised by a high degree of atomic order, resulting in well defined X-ray and electron diffraction peaks, but they lack translational periodicity. This complicates the understanding of the electronic structure and hence of some important physical properties. The unusual electronic transport properties are often traced back to the formation of a pseudogap in the excitation spectrum at the Fermi level[5, 6]. The non-periodicity of the crystal lattice is the reason for special features in the temperature dependence of the thermal conductivity, reflecting a general type of Umklapp scattering[6, 7, 8, 9]. The quasiperiodic atomic arrangement is expected to also influence the magnetic features of quasicrystals (QCs), and in recent years, studies of magnetic properties of QCs have been in the focus of a number of research projects. While the initial studies were mainly performed on metastable Al-Mn QCs [10, 11], a lot of progress has been made since then in preparing stable high-quality ternary QCs with local magnetic moments in alloy systems such as Al-Pd-Mn or Al-Mn-Ge. Depending on structure and stoichiometry, these QCs exhibit ferromagnetism[12], diamagnetism[13], paramagnetism[14, 15] or spin-glass phenomena[16, 17, 18]. Other intensively investigated families of magnetic QCs include Al-Cu-Fe and Al-Co-Ni alloys[19], and the more recently synthesized quasicrystalline compounds containing rare-earth (RE) ions, such as RE-Mg-Zn with well localized $4f$ -electron moments[20, 21, 22, 23].

Several studies of the d -electron magnetism of Mn in icosahedral samples of Al-Pd-Mn have been motivated by the early discovery of the stable icosahedral i -Al-Pd-Mn phase. In spite of the above mentioned variety of magnetic properties found in these QCs, they seem to exhibit the common feature of only a small fraction of the manganese ions carrying a magnetic moment[14, 17]. In some cases this fraction even seems to decrease with decreasing temperature[14]. Theoretical studies and band-structure calculations aimed at explaining the phenomenon that only a fraction of the Mn ions carries a magnetic moment[24], and to relate it to the Hume-Rothery type pseudo gap in the electronic spectrum around the Fermi level[25].

In comparison with the icosahedral Al-Pd-Mn alloys, the situation is less clear for decago-

nal Al-Pd-Mn alloys. For the latter, a larger number of sites has been predicted to carry a moment which, however, is smaller than the Mn moment established in icosahedral compounds[25]. The present work reports the results of measurements of the dc magnetic susceptibility and of ^{27}Al - and ^{55}Mn -NMR studies of the decagonal QC $d\text{-Al}_{69.8}\text{Pd}_{12.1}\text{Mn}_{18.1}$. From our results we infer that the Mn-moments in this compound are distributed very inhomogeneously. In the paramagnetic state and above 100K, only about half of the Mn ions carry a magnetic moment. The data also indicate that the fraction of Mn moments may even decrease upon reducing the temperature below 100K. Finally we confirm the previously reported spin-glass transition at $T_f = 12\text{K}$ [26].

B. The Sample

A metastable icosahedral sample of Al-Pd-Mn was obtained by spinning a melt of the stoichiometric composition of the decagonal phase $\text{Al}_{69.8}\text{Pd}_{12.1}\text{Mn}_{18.1}$ onto a fast turning (30m/s), water cooled Cu wheel. Annealing the resulting tapes with the icosahedral phase for 100 hours at about 820°C transforms them into polycrystalline flakes of the stable decagonal phase[27]. Decagonal Al-Pd-Mn has a columnar structure arranged on a two-dimensional quasiperiodic lattice. The translational period of length $d = 12.56\text{\AA}$ is built up by two different types of layers: a puckered layer P and a flat layer F[3]. The ratio of Al in P to Al in F is approximately 2:1; for Mn this ratio is about 1:8[2].

High resolution transmission electron microscopy confirmed that our sample consists of polycrystalline $d\text{-Al}_{69.8}\text{Pd}_{12.1}\text{Mn}_{18.1}$ with no linear phason strains. Selected area electron diffraction from room temperature down to below 30K proved the high perfection of the decagonal symmetry in the planes and the periodicity along the c -axis(see figure 1). Scanning electron microscopy sets the upper limit of the admixture of a second phase, i.e., $\text{Al}_{11}(\text{Mn},\text{Pd})_4$ on the surface of the back side of the tapes, to about 1%.

C. Experimental Results and their Analysis

1. Magnetic Susceptibility

We measured the dc-susceptibility $\chi(T)$ of $d\text{-Al}_{69.8}\text{Pd}_{12.1}\text{Mn}_{18.1}$ with a dc-SQUID magnetometer between 340K and 2K, and at different magnetic fields between 50G and 5.5T.

Figure 2 shows the inverse susceptibility $1/(\chi(T) - \chi_0)$ measured at 500G between 5K and 350K. As may be seen in the inset of figure 2, field-cooled (FC) and zero-field cooled (ZFC) data differ below $T_f \approx 12$ K. There is a well-defined maximum for the ZFC $\chi(T)$ at T_f . This behaviour confirms a spin-glass type freezing of the Mn-moments, previously claimed from the analysis of ac-susceptibility and specific-heat results measured on the same sample[26]. Above 120K, $\chi(T)$ may be approximated by $\chi(T) = C/(T - \Theta) + \chi_0$ with

$$C = N_A c p^2 \frac{\mu_B^2}{3k_B}, \quad (1)$$

where N_A is Avogadro's number, c the concentration of magnetic ions, and p their effective moment $p = g(JLS)\sqrt{J(J+1)}$. The susceptibility data in the temperature range between 120K and 350K are best approximated with the parameters $C = 0.544$ [emu/mol], $\Theta = -20$ K, and $\chi_0 = -2.45 \cdot 10^{-8}$ [emu/g].

The negative paramagnetic Curie temperature Θ indicates a predominant antiferromagnetic coupling between the Mn d -moments. The Curie constant C implies that $p\sqrt{c} = 2 \pm 0.1\mu_B$ per Mn-atom. This is not compatible with the assumption that all Mn ions adopt a well-defined and identical ionic configuration. If we assume, for example, localized Mn moments, our result for $\chi(T)$ imply a concentration of only $16.5 \pm 0.5\%$ of Mn^{3+} , or $12.5 \pm 0.5\%$ of Mn^{2+} . As we shall see in section C 2, however, about half of the Mn ions carry a magnetic moment, and the distribution of the magnetic sites in d -Al-Pd-Mn is very inhomogeneous. Distinct deviations of $\chi(T)$ from the Curie-Weiss behaviour below 60K (see main frame of figure 2) signal precursor effects of the spin-glass freezing of the Mn moments.

Below 50K the susceptibility is field-dependent in fields below 5T. Figure 3 displays the magnetization $M(H)$ measured at various temperatures. As expected from the $\chi(T)$ data there is a hysteresis at 5K, due to "memory effects" in the spin-glass phase. There is no visible hysteresis in the magnetization loop at 10K, suggesting that the relaxation of the magnetization at that temperature is faster than the time scale of the stepwise variation of the applied magnetic field in our experiments.

2. NMR spectra

We recorded ^{27}Al and ^{55}Mn NMR spectra between room temperature and 8K and at the frequencies of 21, 25, 30, 58, and 70MHz, using standard $\pi/2$ - τ - π spin-echo sequences. Figure

4 shows two spectra recorded at 79 and 140K, respectively, with an excitation frequency of 24.97MHz. The NMR signal is distributed over a wide range of resonant fields from 2.1 to 2.4T. The prominent peaks near 2.25T represent the central ^{27}Al Zeeman transition ($1/2 \leftrightarrow -1/2$). The broad distribution of quadrupolar wings is a generic feature of QCs[28]. The vertical dotted line in Figure 4 indicates the position of the resonance of ^{27}Al nuclei in an aqueous AlClO_3 solution at room temperature and 24.97MHz, which is used as a reference signal. The solid lines represent the results of a computer simulation of the spectra which is described below.

The ^{27}Al central transition is very broad, almost a factor of 10 broader than expected from considering the second order quadrupolar perturbation of the Zeeman line and than the analogous signals observed for the case of the non-magnetic Al-Pd-Re-compounds[28]. The line-width increases with decreasing temperature and, as we shall see below, the peculiar shape of the central line does not arise from anisotropies in the Knight-shift or quadrupolar effects. We argue that this signal consists of two partially resolved contributions representing the central transitions of Al nuclei located in either of two distinctly different local environments. One of the contributions, denoted as line I in figure 4, has very small or zero line-shift, while the other, denoted as line II in figure 4, exhibits a relatively large and T -dependent negative shift.

In order to confirm this conjecture we have looked for and found appreciable differences in the spin-spin relaxation for the ^{27}Al nuclei that were allocated to different environments. This was achieved by changing τ in the $\pi/2 - \tau - \pi$ echo sequence. Figure 5 displays two spectra recorded at 24.97MHz and 96K with two different values for τ . The spectrum with $\tau = 30\mu\text{s}$ shows a distinct shoulder on the high-field side while in the spectrum with $\tau = 180\mu\text{s}$ this feature is clearly absent. In the upper inset of figure 5 we display the difference of the two spectra after taking into account T_2^* -effects ($1/T_2^* = 1/T_1 + 1/T_2 \approx 1/T_2$). These effects affect both, line I and line II, which experience a suppression of signal intensity due to transverse relaxation processes. The loss of signal due to these processes has been taken into account by weighing factors obtained from a fit of $A \cdot e^{\frac{-2\tau+d_2}{T_{2,I}^*}} + B \cdot e^{\frac{-2\tau+d_2}{T_{2,II}^*}}$ to the echo intensity as a function of τ , with d_2 as the duration of the π -pulse. The thus obtained difference of the two spectra then reveals a clear manifestation of line II. The solid lines in the inset as well as in the main frame display the results of computer simulations, briefly discussed below. We conclude that the agreement between the experimental data and the calculated curves

provides strong evidence for the existence of two different types of environments for the Al nuclei, giving rise to signals I and II, respectively.

Support for our claims is obtained from the results of our computer simulations of NMR spectra measured in a wide range of T -, H - and τ -values. The NMR frequency of a nucleus depends on the local magnetic field and on the local electric field gradient at the position of the nucleus, such that

$$\nu = \nu_L - \nu_Q \left(m - \frac{1}{2}\right) \frac{3\cos^2\theta - 1}{2}, \quad (2)$$

where ν_L and ν_Q denote the Larmor and the quadrupolar frequency, respectively, m is the z -component of the upper nuclear spin state of the transition, and θ is the angle between the principal axis of the field gradient with respect to the local magnetic field at the position of the nucleus. We assumed that the Larmor frequencies ν_L obey a Gaussian distribution whose width w is caused by a (T -dependent) distribution of shifts, centered around ν_0 . Our previous attempts for fitting the – much simpler – ^{27}Al -spectra of non-magnetic icosahedral quasicrystals of the Al-Pd-Re-family were successful when choosing the quadrupolar frequency ν_Q to be uniformly distributed between some hundred kilohertz and a few megahertz. In the simulated ^{27}Al -spectra of the present work, this distribution of ν_Q ranges from 200kHz to 2MHz. The experimental spectra were successfully fitted by assuming two different sets of environments, characterized by two Gaussian distributions with different widths, w_I and w_{II} , spread around two different central frequencies $\nu_{0,I}$ and $\nu_{0,II}$. The distribution of ν_Q cited above was assumed to be the same for both environments. Figure 6 shows the calculated three contributions to the total spectrum, i.e., line I and line II of ^{27}Al in the two different environments, and the signal originating from nuclei of non-magnetic Mn ions (discussed below). In order to compare the simulated spectra with the experimental data, the frequencies were translated into the corresponding applied fields. The distribution of angular orientations of the local quadrupolar axes was assumed to be random, because we used a polycrystalline sample.

3. NMR line shifts and widths

We determined the shift ΔH_{II} of line II by means of both, computer simulations of signals obtained with $\tau = 30\mu\text{s}$, and also by subtracting the spectrum monitored with a

long τ from that recorded with a short τ , both at the same temperature, of course. Figure 7 shows the relative line-shift $K_{\text{II}} := \Delta H_{\text{II}}/H$ of line II as a function of temperature. The open symbols indicate the values obtained by subtraction, the closed symbols correspond to values obtained by computer simulations. The absolute line shifts ΔH scale linearly with field and can be expressed by

$$K := \frac{\Delta H}{H} = K_{\text{ce}} + K_{\text{mag}}(T), \quad (3)$$

where K_{ce} is a temperature-independent contribution, which in our case is much larger in magnitude than those found in non-magnetic quasicrystals[14, 28, 29]. Temperature-independent NMR line-shifts can be caused by a variety of processes, however, K_{ce} of line II is too large to be attributed to typical chemical shifts or to quadrupolar effects. Therefore one is tempted to associate K_{ce} with the paramagnetism of the conduction electrons. In common metals this contribution, the Knight shift, is positive, but, in our case K_{ce} is negative. A negative and temperature-independent line shift cannot be caused by conduction electrons originating from the Al *s* and *p* shells but may be due to itinerant electrons originating from the Mn *d*-shell[30, 31]. The Pd *d*-band is full and therefore these states are not expected to contribute significantly to the resonance shift. Such an interpretation is compatible with recent experimental results concerning the electronic structure of Al-Pd-Mn quasicrystals [32]. Nevertheless, the origin of the negative Knight-shifts, also found in other quasicrystals, is still an open question. For line I the relative shift K is also negative but less than 100ppm. The existence of two distinct lines with different shifts therefore strongly suggests that the conduction electron density at the ^{27}Al nuclei is not uniform. In some regions, which contribute to the intensity of line II, there is a substantial conduction electron density and, as we argue below, the Mn ions in that region are magnetic. In other regions, which contribute to the intensity of line I, the conduction-electron density is reduced and the Mn ions are non-magnetic.

$K_{\text{mag}}(T)$, only clearly observed for line II, exhibits a Curie-Weiss type behaviour in the whole temperature range covered by the data shown in figure 7. The paramagnetic Curie-temperature $\theta = -6\text{K}$ is in fair agreement with the value obtained from fits to the susceptibility. The inset of figure 7 displays the line-shift data plotted versus the dc-susceptibility

measured in different fields. It confirms that $K_{\text{mag}}(T)$ may be written as

$$K_{\text{mag}}(T) = A \cdot \chi(T). \quad (4)$$

The proportionality constant A is a measure of the average coupling strength of the ^{27}Al nuclear spins to the Mn magnetic moments. For metals, A is usually written as

$$A = \frac{1}{\mu_B N} H_{\text{eff}}, \quad (5)$$

with H_{eff} as the hyperfine field from each aligned Bohr magneton. N is Avogadro's number[31]. In our case, where only a fraction c of the Mn ions is magnetic and because the molar susceptibility is calculated per total Mn content, equation (5) has to be changed to

$$A = \frac{1}{\mu_B c N} H_{\text{eff}}. \quad (6)$$

In spite of the large error bars, our data suggest that there are two temperature regimes with different values of A , below and above approximately 110K. This change may simply reflect a reduction of the fraction of magnetic Mn moments c . This interpretation gains support from the ^{55}Mn NMR spectra, where we observe that the intensity of the *non-magnetic* Mn line is 35% and 50% of the total expected Mn intensity above and below 100K, respectively. However, other processes leading to a change in the hyperfine coupling cannot be ruled out.

The widths of both lines increase with decreasing temperature and therefore give a clear indication that they are both of magnetic origin. Also line I is much broader than the central ^{27}Al line in other Al-Pd-Mn compounds[14], suggesting that the regions of the two environments mentioned above are finely dispersed in the bulk of the sample. At this point we focus our attention on line II, where the influence of the Mn moments is particularly pronounced. In figure 8 the temperature dependence of the ratio $w_{\text{II}}/\nu_{\text{irrad}}$, where w_{II} is again the width of line II and ν_{irrad} the corresponding irradiation frequency, is plotted for four different irradiation frequencies, i.e., four different average applied fields. Since all the data fall onto a single curve, it follows that the line-width scales with the irradiation frequency, or, equivalently, with the applied magnetic field and, therefore, must be of magnetic origin. The enhancement with decreasing temperature occurs with increasingly negative slope. The inset of figure 8 displays the same data plotted versus the dc-susceptibility measured at

similar fields. The width of line II originates from a distribution of shifts of the ^{27}Al nuclei around an average shift. The slope of that curve therefore is a measure of the width of the distribution of the site dependent coupling strengths $A(\mathbf{r})$ between the Al nuclear spins of line II and the Mn moments, with respect to the total magnetic susceptibility, which is mainly due to localized Mn moments. It shows a pronounced change at approximately 110K. Such a slope change could be induced by a reduction of the number of magnetic Mn ions, leading to a reduced increase in the susceptibility.

The NMR spectra recorded at a chosen frequency reveal some additional intensity at a field where one expects the ^{55}Mn signal at zero shift. This is most clearly seen near 5.5T in figure 6. Since the hyperfine field coupling of the Mn moment to the nucleus of the same ion is through the core-polarization, which is of the order of $-100\text{kG}/\mu_B$ for Mn[11], even a small moment on a Mn ion would shift its resonance frequency by several MHz. Therefore this signal intensity in our spectra must originate from non-magnetic Mn atoms (see figure 6). From the spectra recorded at 70MHz, where the Mn-signal is clearly resolved, we conclude that the fraction of Mn-atoms carrying no magnetic moment is of the order of $45\pm 15\%$. We note that this value is not far from the ratio of the intensities of line I and II which was found to be 0.4 ± 0.1 . Thus we may again conclude that the Al lines I and II arise from Al nuclei in the neighborhood of nonmagnetic and magnetic Mn ions, respectively. Considering the average moment of $p = 2 \pm 0.1\mu_B$, deduced from the dc molar susceptibility data with respect to the total Mn content, we estimate that the average effective moment per magnetic Mn ion is $p = 3\mu_B$, if we assume that 45% of the Mn ions actually are magnetic. This number is not compatible with any of the possible ionization states of Mn, which would lead to $p = 4\mu_B$ for Mn^{4+} , $p = 5\mu_B$ for Mn^{3+} , and $p = 5.9\mu_B$ for Mn^{2+} .

4. NMR Spin-lattice relaxation rate

We measured the spin-lattice relaxation rate T_1^{-1} of line I from room temperature down to 15K in three different applied fields. The values of T_1 were extracted from fits to the nuclear magnetization recovery $m(t)$, which was first destroyed using a long comb of rf-pulses, followed by a variable delay t and a spin-echo sequence $\pi/2 - \tau - \pi$ with a long $\tau = 180\mu\text{s}$. In this manner it is possible to identify exclusively the spin-lattice relaxation rate related to line I. Using shorter values of τ in these measurements leads to changes in

$m(t)$ which, in our view, results in less reliable values of T_1 . According to standard NMR theory, the signal intensity of the central line of a spin $I = 5/2$ nucleus relaxes such that[33]:

$$1 - m(t)/m(\infty) = 0.4762e^{-15t/T_1} + 0.2667e^{-6t/T_1} + 0.2571e^{-t/T_1}. \quad (7)$$

Even for line I alone, there is no distinct single Al-site, but rather a variety of sites leading to a distribution of T_1 's. Since the details of the distribution of T_1 's are not known, we simply model $m(t)$ by replacing the exponentials by stretched exponential functions[37]:

$$1 - m(t)/m(\infty) = 0.4762e^{-15(t/T_1)^\beta} + 0.2667e^{-6(t/T_1)^\beta} + 0.2571e^{-(t/T_1)^\beta}. \quad (8)$$

Figure 9 displays an example of a magnetization recovery at a relatively low temperature and the corresponding best fit to the data using equation (8). With an increasing pulse separation τ in the echo sequence the exponent β converges to an approximate value of 0.9. Therefore, in the subsequent analysis we set $\beta = 0.9$. As may be seen in the inset of figure 9, also the T_1 values turned out to vary with τ but to reach a constant value for $\tau \geq 180\mu\text{s}$. Therefore, we fixed τ to $180\mu\text{s}$ for all the measurements of T_1 discussed below.

Figure 10 displays $T_1^{-1}(T)$ obtained from fitting the data obtained at three different fields of 5.2T, 2.25T, and 1.85T, with $\tau = 180\mu\text{s}$ to equation (8). Below 50K the spin-lattice relaxation rate increases with an increasingly negative slope as T approaches the spin-glass freezing temperature T_f . This behaviour is typical for nuclear spins which experience the influence of magnetic moments that undergo a gradual slowing down of their fluctuations. In the present case, the Mn moments, although predominantly affecting line II, are also felt in the relaxation of the nuclear spins contributing to line I, as the spin-glass transition is approached upon cooling. At high temperatures, the spin-lattice relaxation rate of non-magnetic nuclei due to paramagnetic centers is given by[34]:

$$\frac{1}{T_1} = C \frac{\tau}{1 + \omega_I^2 \tau^2}. \quad (9)$$

C is proportional to the hyperfine-field coupling between the Mn moments and the Al nuclei, τ is the correlation time of the Mn moments, and $\omega_I = 2\pi\nu_{0,I}$ is the Larmor precession frequency of the nucleus under investigation[38]. In the fast-motion regime, at temperatures much higher than T_f , $\omega_I^2 \tau^2$ is much smaller than 1 and the relaxation rate is temperature- and field-independent. As T is reduced towards T_f , the moment fluctuations slow down

and cause an increase of $T_1^{-1}(\propto \tau)$, as observed below 50K. The τ -driven increase can be understood by assuming that $\omega^2\tau^2$ is still much less than 1, which is implicitly confirmed by the almost H -independent increase of $T_1^{-1}(T)$ below 50K. Close to T_f , the growing linewidth usually prohibits to extract reliable T_1 values. In our case this is true for $T < 20$ K.

The $T_1^{-1}(T)$ plot in figure 10 exhibits a broad maximum centered around 120K. This maximum is very unusual and has – to our knowledge – never been seen in $T_1^{-1}(T)$ of any other quasicrystalline compound. The spin-lattice relaxation rate usually contains three contributions

$$T_1^{-1} = T_{1,ce}^{-1} + T_{1,mag}^{-1} + T_{1,q}^{-1}. \quad (10)$$

The total relaxation is characterized by $T_{1,ce}^{-1}$, due to conduction electrons, $T_{1,mag}^{-1}$ reflecting the relaxation due to the paramagnetic centers, and $T_{1,q}^{-1}$ capturing the quadrupolar relaxation. In a simple metal, $T_{1,ce}^{-1}$ is known to vary linearly with temperature. In quasicrystals the relaxation due to itinerant electrons depends on the shape of the density of states at the Fermi level and thus on the shape of the pseudogap. A power-law or polynomial increase of the spin-lattice relaxation rate with rising temperature is expected[5, 28]. It may be seen in figure 10 that above 175K the T -dependence of the spin-lattice relaxation rate may well be dominated by conduction electrons and they still contribute significantly to the total T_1^{-1} in the crossover regime around 120K. However $T_{1,ce}^{-1}$ cannot account for the maximum at 120K, unless some anomaly in the electronic excitation spectrum causes the feature at that temperature. Major changes in $T_{1,ce}$ around 120K are, however, not to be expected because the monotonous variation of the electrical resistivity with temperature, shown in figure 11, does not support a corresponding feature in the electronic excitation spectrum that would cause the anomaly in T_1^{-1} around 120K.

Also any substantial contribution of $T_{1,q}^{-1}$ can be ruled out. The spin-lattice relaxation rate of Al nuclei is larger by more than a factor of 10 in d -Al-Pd-Mn than it is in i -Al-Pd-Re, where it is still dominated by $T_{1,ce}^{-1}$ and not $T_{1,q}^{-1}$ [5]. Hence $T_{1,q}^{-1}$ in d -Al-Pd-Mn is expected to be very small in comparison with other contributions, unless a major change of structure at some temperature occurs in that compound. Results of selected area electron diffraction (SAED) measurements from room temperature down to below 30K indicate that no structural changes occur in this temperature regime and therefore it may be concluded that $T_{1,q}^{-1}$ does not contribute significantly to changes in $T_1^{-1}(T)$.

We are thus left with the second significant term in (10), i.e. $T_{1,\text{mag}}^{-1}$, which describes the magnetic interactions between the Al nuclear spins and the Mn d -moments. In our case, with $\omega_1\tau \ll 1$ in equation (9), T_1^{-1} is expected to be almost T - and H -independent. We note that the values of T_1^{-1} of other magnetic quasicrystals of the Al-Cu-Fe-family[5, 35] and icosahedral samples of Al-Pd-Mn with lower Mn concentration[14] are smaller than for the presently investigated material by at least one order of magnitude as well. This giant difference is mainly attributed to the larger contribution of $T_{1,\text{mag}}^{-1}$ to the total spin-lattice relaxation rate in the present case. Based on these arguments we suggest that the maximum in $T_1^{-1}(T)$ is related to $T_{1,\text{mag}}^{-1}(T)$ and reflects the previously mentioned reduction of the concentration of magnetic Mn moments below approximately 100K.

In figure 12 we compare the low temperature ^{27}Al spin-lattice relaxation rate of d -Al-Pd-Mn with those of ^{27}Al nuclei in a non-magnetic i -Al-Pd-Re quasicrystal[28] and in i -Al-Pd-Mn[14]. In the covered temperature region the relaxation rates in both, the non-magnetic i -Al-Pd-Re as well as the weakly magnetic i -Al-Pd-Mn, are smaller by more than an order of magnitude and exhibit a distinctly different temperature dependence.

D. Summary

Our susceptibility data and our NMR spectra reveal that at elevated temperatures more than half of the Mn ions in decagonal $\text{Al}_{69.8}\text{Pd}_{12.1}\text{Mn}_{18.1}$ carry a small magnetic moment, giving rise to an average Mn-moment of $2\mu_B$. These moments experience an average antiferromagnetic interaction, leading to a spin-glass freezing at $T_f \approx 12\text{K}$. We presented arguments that the number of these moments is gradually reduced below 100K. A similar reduction of moments was observed at lower temperatures in i -Al-Pd-Mn with a much smaller density of magnetic Mn moments[14].

The ^{27}Al NMR spectra show two partially resolved lines. Line II is clearly much more influenced by the Mn-magnetism. Similar line-shapes have been found in very early experiments on Mn-rich metastable Al-Mn quasicrystals[11], but they could not be resolved into two lines at that time. We argue that the two lines are due to Al on sites in environments favoring the formation of a magnetic moment on the Mn ions (line II) and to Al in an environment, where the Mn moments are quenched (line I). Our results strongly suggest that simple Al- p -Mn- d hybridization alone may not adequately account for the phenomenon of

Mn-magnetism in QC's, but that a more subtle, conduction-electron mediated long-range mechanism has to be considered [24].

We have not yet found an unequivocal interpretation for the broad maximum of T_1^{-1} at 120K. The same process that leads to that maximum seems to lead to a reduction of the fraction of Mn-ions that carry a magnetic moment, or, possibly an increased hyperfine coupling below 110K. Neither a structural transition nor a significant change in the electronic density of states is indicated by SAED and transport measurements, respectively.

E. Acknowledgement

We thank René Monnier for fruitful discussions, Roland Wessiken for his help with the temperature-dependent selected area electron diffraction, and Matthias Weller for his assistance in the measurement of the electrical conductivity.

-
- [1] D. Shechtman, I. Blech, D. Gratias, and J. W. Cahn, Phys. Rev. Lett. **53**, 1951 (1984).
 - [2] C. Beeli and S. Horiuchi, Phil. Mag. B **70**, 215 (1994).
 - [3] W. Steurer, T. Haibach, B. Zhang, C. Beeli, and H.-U. Nissen, J. Phys.: Condens. Matter **6**, 613 (1994).
 - [4] M. Boudard, M. D. Boissieu, C. Janot, G. Heger, C. Beeli, H.-U. Nissen, H. Vincent, R. Iberson, M. Audier, M. Audier, et al., J. Phys.: Condens. Matter **4**, 10149 (1992).
 - [5] X.-P. Tang, E. A. Hill, S. K. Wonnell, S. J. Poon, and Y. Wu, Phys. Rev. Lett. **79**, 1070 (1997).
 - [6] K. Giannò, A. V. Sologubenko, L. Liechtenstein, M. A. Chernikov, and H. R. Ott, Ferroelectrics **250**, 249 (2001).
 - [7] P. A. Kalugin, M. A. Chernikov, A. Bianchi, and H. R. Ott, Phys. Rev. B **53**, 14145 (1996).
 - [8] M. A. Chernikov, A. Bianchi, E. Felder, U. Gubler, and H. R. Ott, Europhysics Letters **35**, 431 (1996).
 - [9] P. A. Kalugin and A. Katz, Europhys. Lett. **21**, 921 (1993).
 - [10] M. E. McHenry, D. D. Vvendesky, M. E. Eberhard, and R. C. O'Handley, Phys. Rev. B. **37**, 10887 (1988).

- [11] W. W. Warren, H.-S. Chen, and G. P. Espinosa, Phys. Rev. B **34**, 4902 (1986).
- [12] Y. Yokoyama and A. Inoue, Materials Transactions, JIM **37**, 559 (1996).
- [13] F. Hippert, M. Audier, H. Klein, R. Bellissent, and D. Boursier, Phys. Rev. Lett. **76**, 54 (1996).
- [14] J. L. Gavilano, D. Rau, S. Mushkolaj, H. R. Ott, J. Dolinšek, and K. Urban, Phys. Rev. B **65**, 214202 (2002).
- [15] J. Dolinšek, M. Klanjšek, T. Apih, J. L. Gavilano, K. Giannò, H. R. Ott, J. M. Dubois, and K. Urban, Phys. Rev. B **64**, 24203 (2001).
- [16] H. Fujimaki, K. Motoya, H. Yasuoka, K. Kimura, T. Shibuya, and S. Takeuchi, J. Phys. Soc. Jpn. **60**, 2067 (1991).
- [17] M. A. Chernikov, A. Bernasconi, C. Beeli, A. Schilling, , and H. R. Ott, Phys. Rev. B **48**, 3058 (1993).
- [18] J. C. Lasjaunias, A. Sulpice, N. Keller, J. J. Préjean, and M. de Boissieu, Phys. Rev. B **52**, 886 (1995).
- [19] A. Yamamoto, K. Kato, T. Shibuya, and S. Takeuchi, Phys. Rev. Lett. **65**, 1603 (1990).
- [20] I. R. Fisher, K. O. Cheon, A. F. Panchula, P. C. Canfield, M. Chernikov, H. R. Ott, and K. Dennis, Phys. Rev. B **59**, 308 (1999).
- [21] T. J. Sato, H. Takakura, A. P. Tsai, K. Shibata, K. Ohoyama, and K. H. Andersen, Phys. Rev. B **61**, 476 (2000).
- [22] K. Giannò, A. V. Sologubenko, M. A. Chernikov, H. R. Ott, I. R. Fisher, and P. Canfield, Materials Science and Engineering **294-296**, 715 (2000).
- [23] S. Wessel, A. Jagannathan, and S. Haas, arXiv **cond-mat**, 0209405v1 (2002).
- [24] G. T. de Laissardiere and D. Mayou, Materials Science and Engineering **294-296**, 621 (2000).
- [25] J. Hafner and M. Krajčí, Phys. Rev. B **57**, 2849 (1998).
- [26] M. A. Chernikov, C. Beeli, E. Felder, S. Büchi, and H. R. Ott, unpublished (2000).
- [27] C. Beeli, P. Stadelmann, R. Lück, and T. Gödecke, Proc. 5th int. conf. quasi. **ICQ 5**, 680 (1995).
- [28] J. L. Gavilano, B. Ambrosini, P. Vonlanthen, M. A. Chernikov, and H. R. Ott, Phys. Rev. Lett. **79**, 3058 (1997).
- [29] T. Apih, M. Klanjšek, D. Rau, and J. Dolinšek, Phys. Rev. B **61**, 11213 (2000).
- [30] A. M. Clogston, V. Jaccarino, and Y. Yafet, Phys. Rev. **134**, A650 (1964).

- [31] G. C. Carter, L. H. Bennett, and D. J. Kahan, *Metallic Shifts in NMR* (Pergamon, Oxford, 1977).
- [32] M. Erbudak, A. Hensch, J. Keller, B. Roessner, and A. R. Kortan, Journal of electron spectroscopy **120**, 47 (2001).
- [33] A. Narath, Phys. Rev. **162**, 320 (1967).
- [34] A. Abragam, *Principles of Nuclear Magnetism* (Oxford Science Publications, 1994).
- [35] J. Dolinšek and M. Klajnšek, Phys. Rev. B **63**, 134203 (2001).
- [36] A. Bianchi, F. Bommeli, M. A. Chernikov, U. Gubler, L. Degiorgi, and H. R. Ott, Phys. Rev. B **55**, 5730 (1997).
- [37] We found good agreement between equation (8) and magnetization recoveries obtained by computer simulations of a collection of ensembles with different T_1 .
- [38] Equation (9) is a high-temperature approximation where the correlations among the paramagnetic moments are neglected[34].

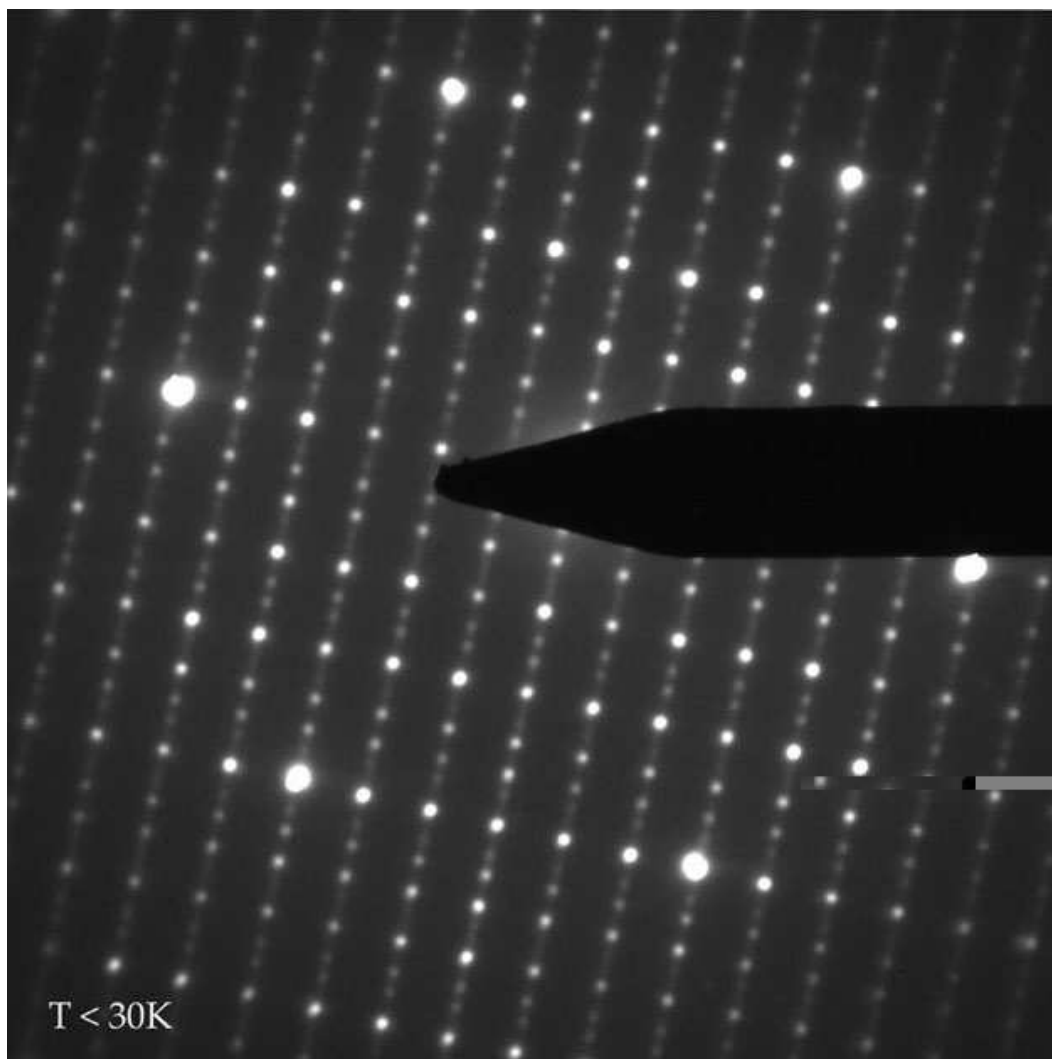


FIG. 1: Selected area electron diffraction (SAED) picture of *d*-Al-Pd-Mn at 30K

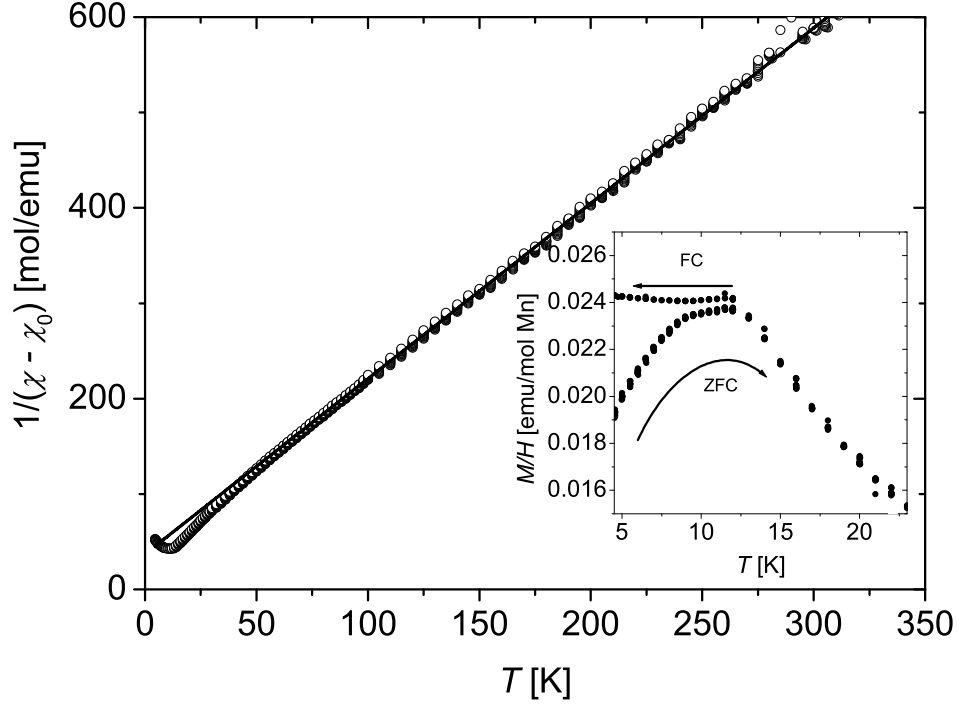


FIG. 2: The inverse dc susceptibility $\chi(T)$ after subtracting a constant negative offset per mol of Mn in an applied field of 500G. The solid line represents the high-temperature Curie-Weiss fit. The inset displays the dc susceptibility below 24K. Below $T_f = 12\text{K}$ the zero field cooled data deviates from the temperature independent field cooled data.

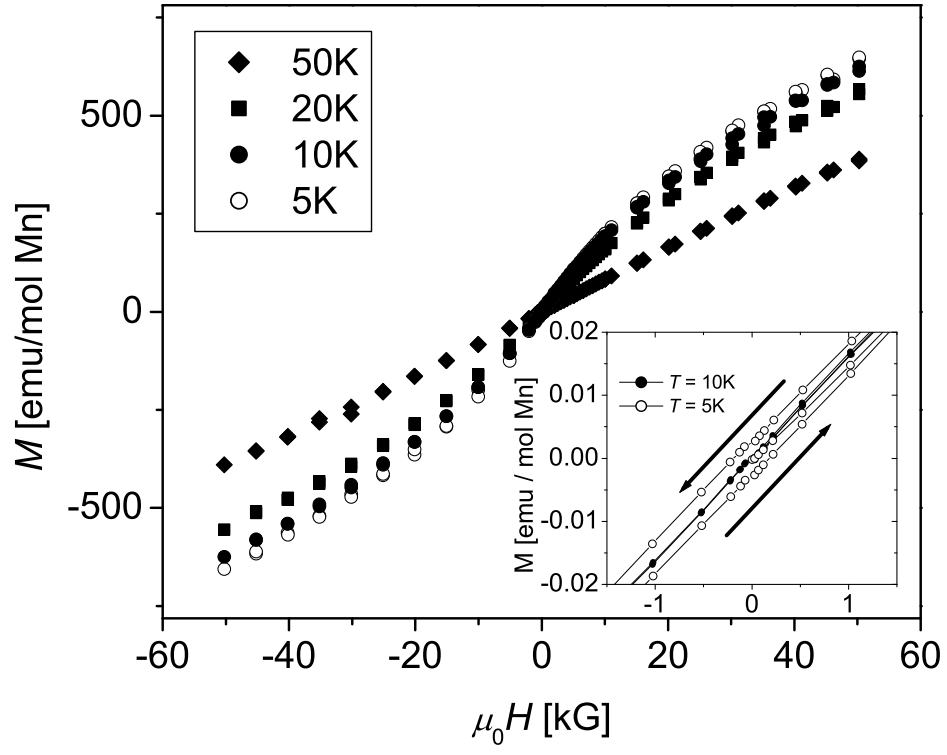


FIG. 3: Magnetization $M(H)$ at various temperatures. Only the data at 5K shows a small hysteresis, visible in the $M(H)$ -curves in the inset.

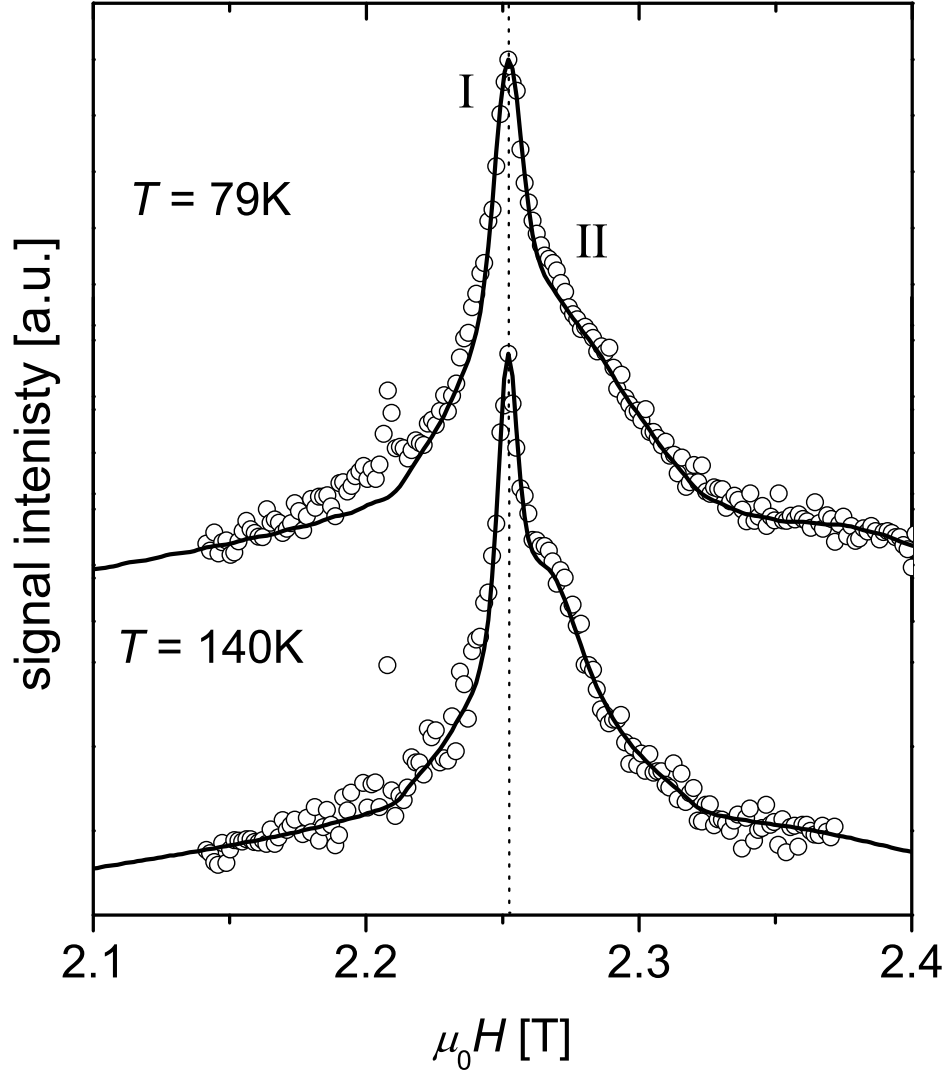


FIG. 4: ^{27}Al NMR spectra of $d\text{-AlPdMn}$ at 24.97 MHz with $\tau = 30\mu\text{s}$. The vertical dotted line indicates the position of the ^{27}Al line in an aqueous solution of AlClO_3 . The solid lines result from computer simulations of the spectra (see text). The narrow signal at 2.207 T arises from the ^{63}Cu nuclei of the measurement coil.

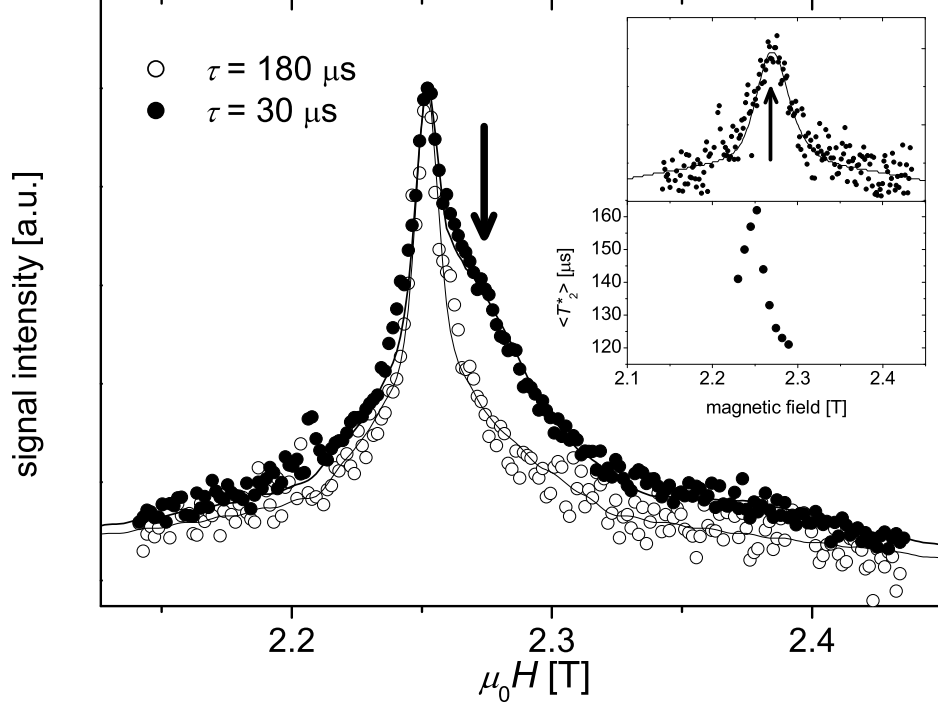


FIG. 5: ^{27}Al and ^{55}Mn NMR spectra of $d\text{-AlPdMn}$ at 24.97 MHz and 96 K with $\tau = 30\mu\text{s}$ and $\tau = 180\mu\text{s}$. The arrow indicates the center of line II which is also indicated by an arrow in the upper inset. The upper inset displays the difference between the spectra at $180\mu\text{s}$ and $30\mu\text{s}$, after taking T_2^* -effects into account. The solid line in the inset is the contribution of Line II to fitting the set of data represented by the full circles in the main frame. The lower inset presents the average spin-spin relaxation rate $\langle T_2^* \rangle$ over the central part of the spectra. The excess signal at 2.207 T again arises from the ^{63}Cu nuclei of the measurement coil. For the definition of T_2^* see text.

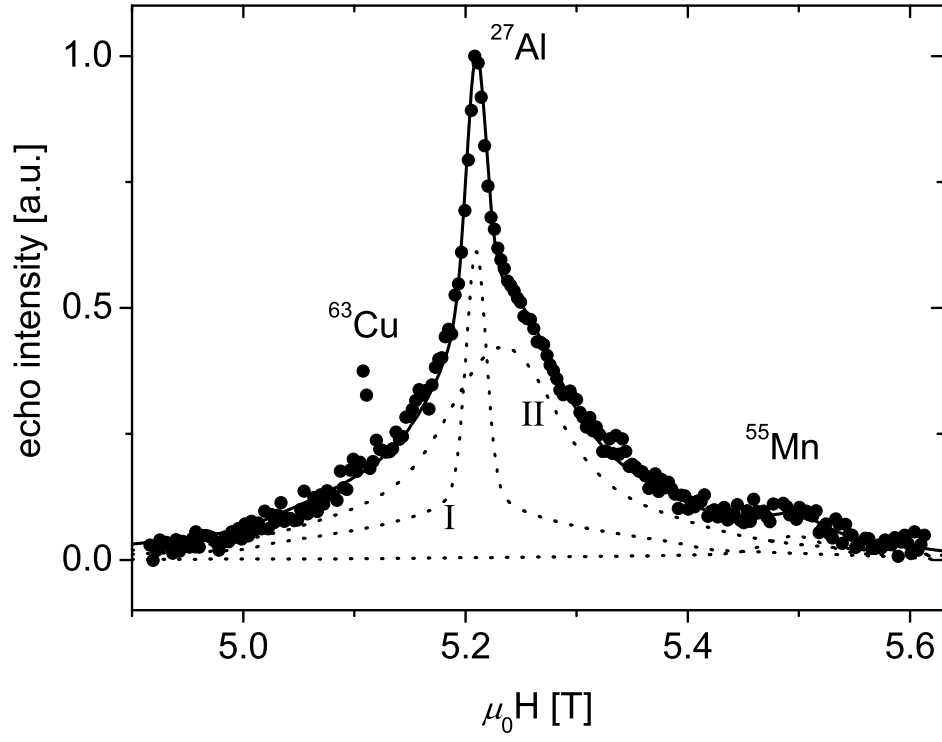


FIG. 6: ^{27}Al and ^{55}Mn NMR spectrum of *d*-AlPdMn at 57.8MHz and 101K. The solid line represents a fit to the data, the dotted lines indicate the individual contributions of line I, line II and the Mn-signal.

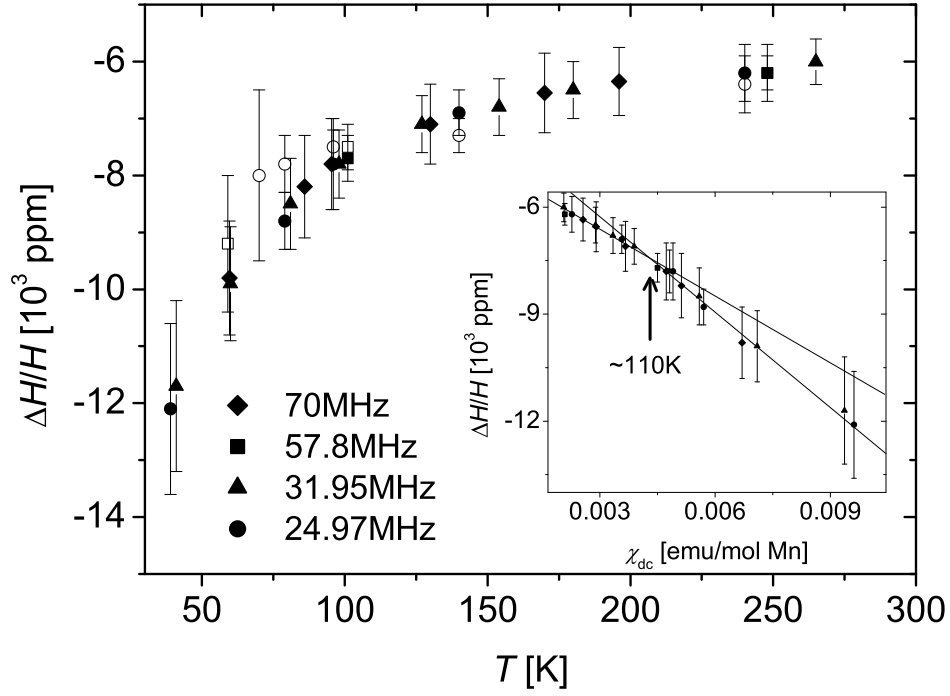


FIG. 7: Temperature-dependence of the relative ^{27}Al line-shifts $\Delta H/H$ of line II in $d\text{-AlPdMn}$ at various fields. The open symbols are values obtained from the difference of the lines recorded with $\tau = 30\mu\text{s}$ and $\tau = 180\mu\text{s}$, respectively. The closed symbols are values obtained from fits to the spectra. The inset shows the line-shifts plotted versus the dc-susceptibility. There is a slight change of slope at approximately 110K, indicated by the two lines and the arrow.

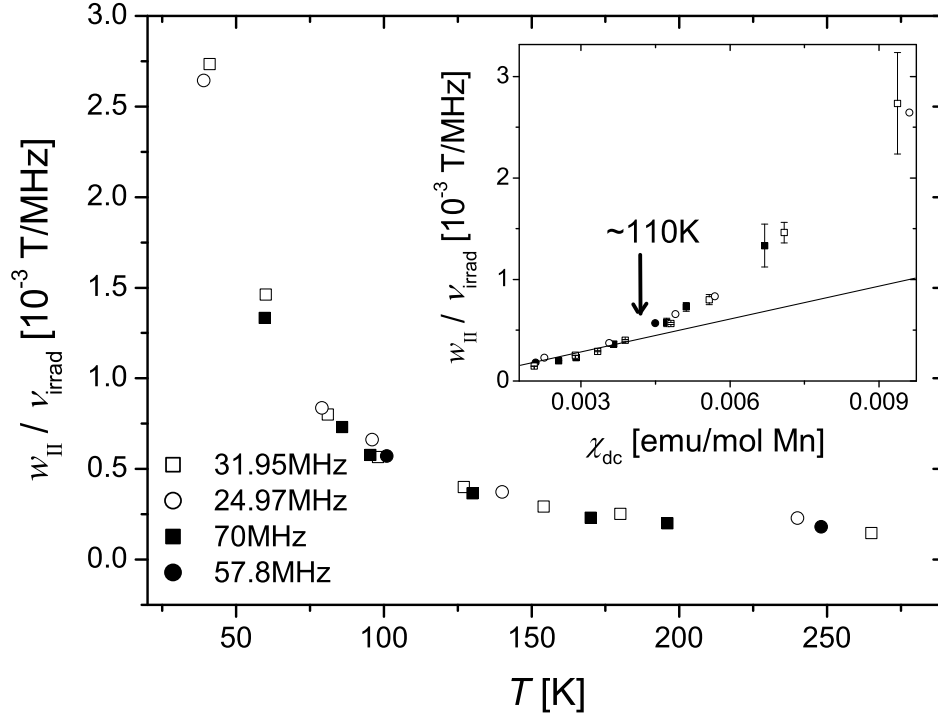


FIG. 8: Temperature-dependence of the width of line II divided by the irradiation frequency ν_{irrad} . The inset shows the same ratio plotted versus the dc-susceptibility. There is a pronounced change of slope at approximately 110K, indicated by the arrow. The solid line fits the data at elevated temperatures.

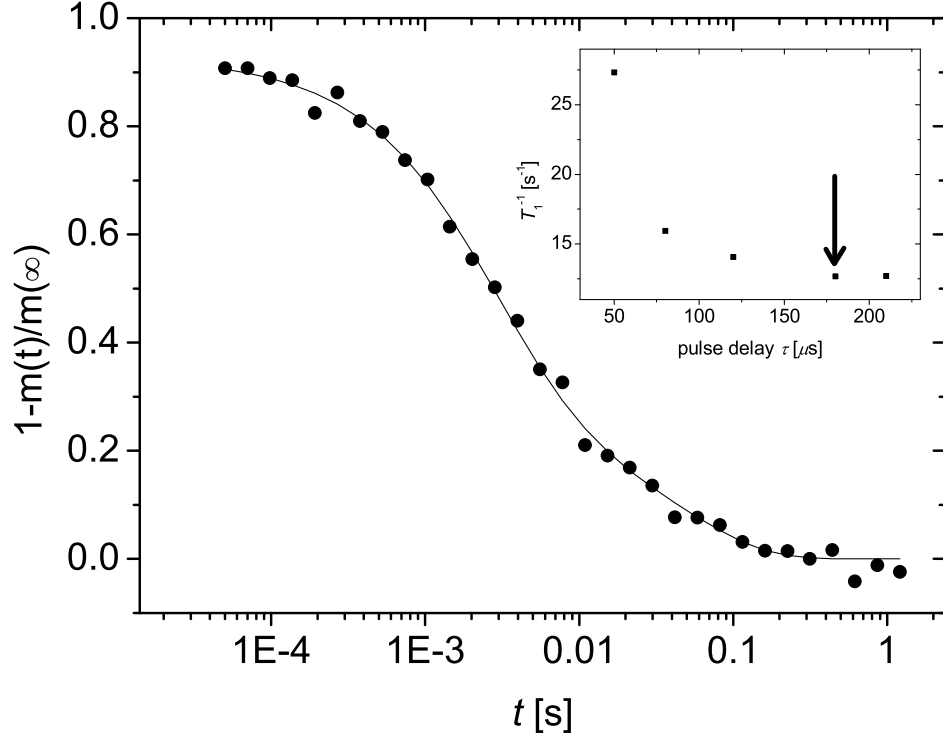


FIG. 9: Magnetization recovery curve related with line I at 57.8MHz and 24.5K. The solid line represents a fit to equation (8). The inset displays how $T_1^{-1}(68\text{K})$ saturates with increasing τ . The arrow marks $\tau = 180\mu\text{s}$, the pulse delay that was used in our measurements.

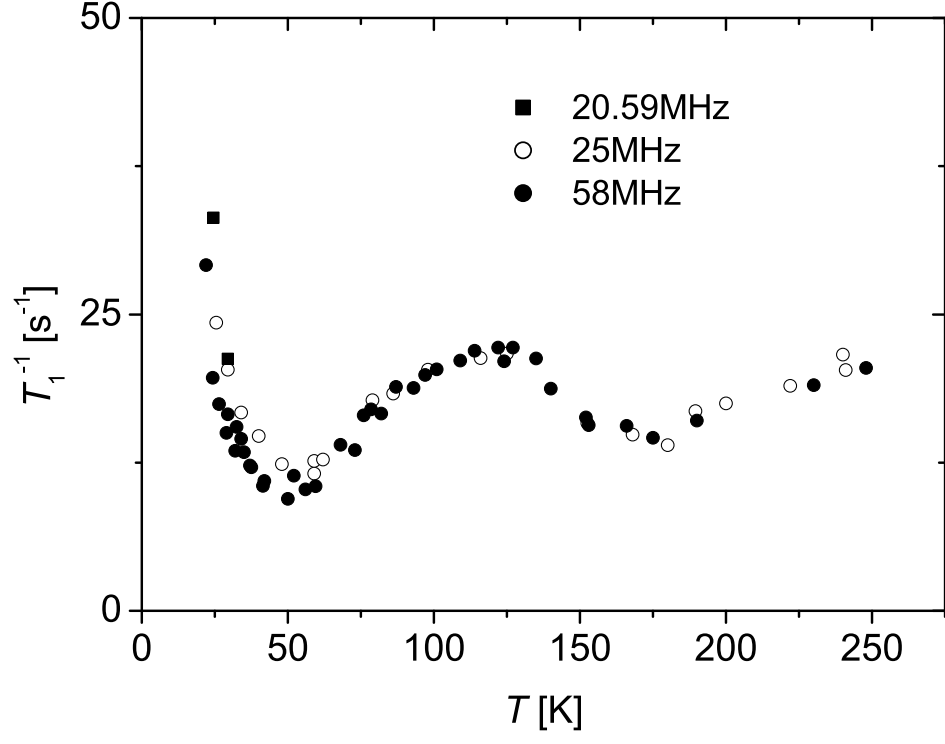


FIG. 10: Spin-lattice relaxation rate $T_1^{-1}(T)$ for line I between 25 and 250K.

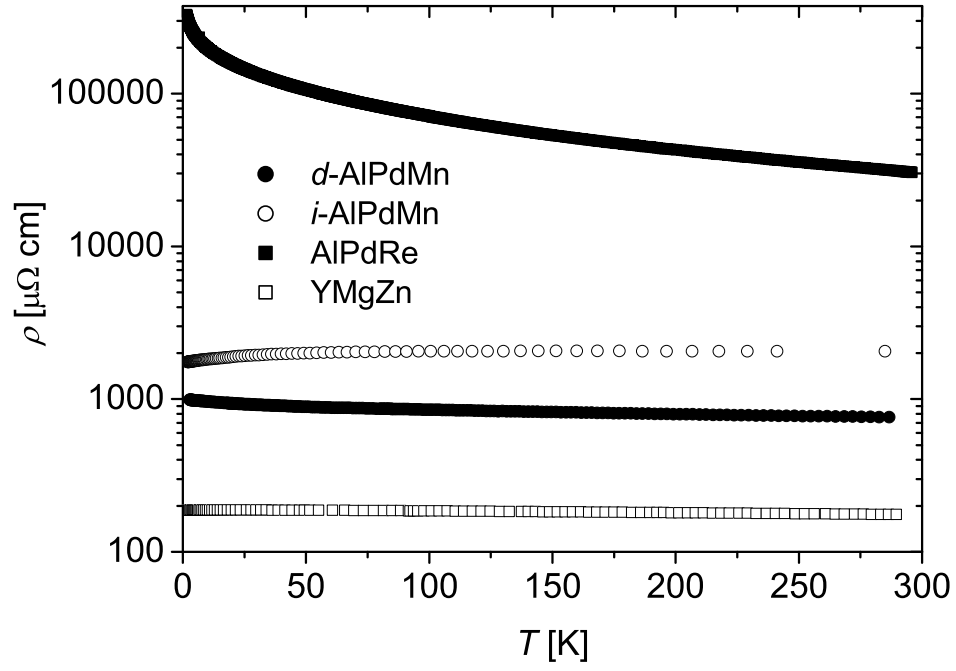


FIG. 11: Zero-field electrical resistivity $\rho(T)$ of d -Al-Pd-Mn compared to $\rho(T)$ of i -Al-Pd-Mn [15], i -Al-Pd-Re[36], and Y-Mg-Zn[22].

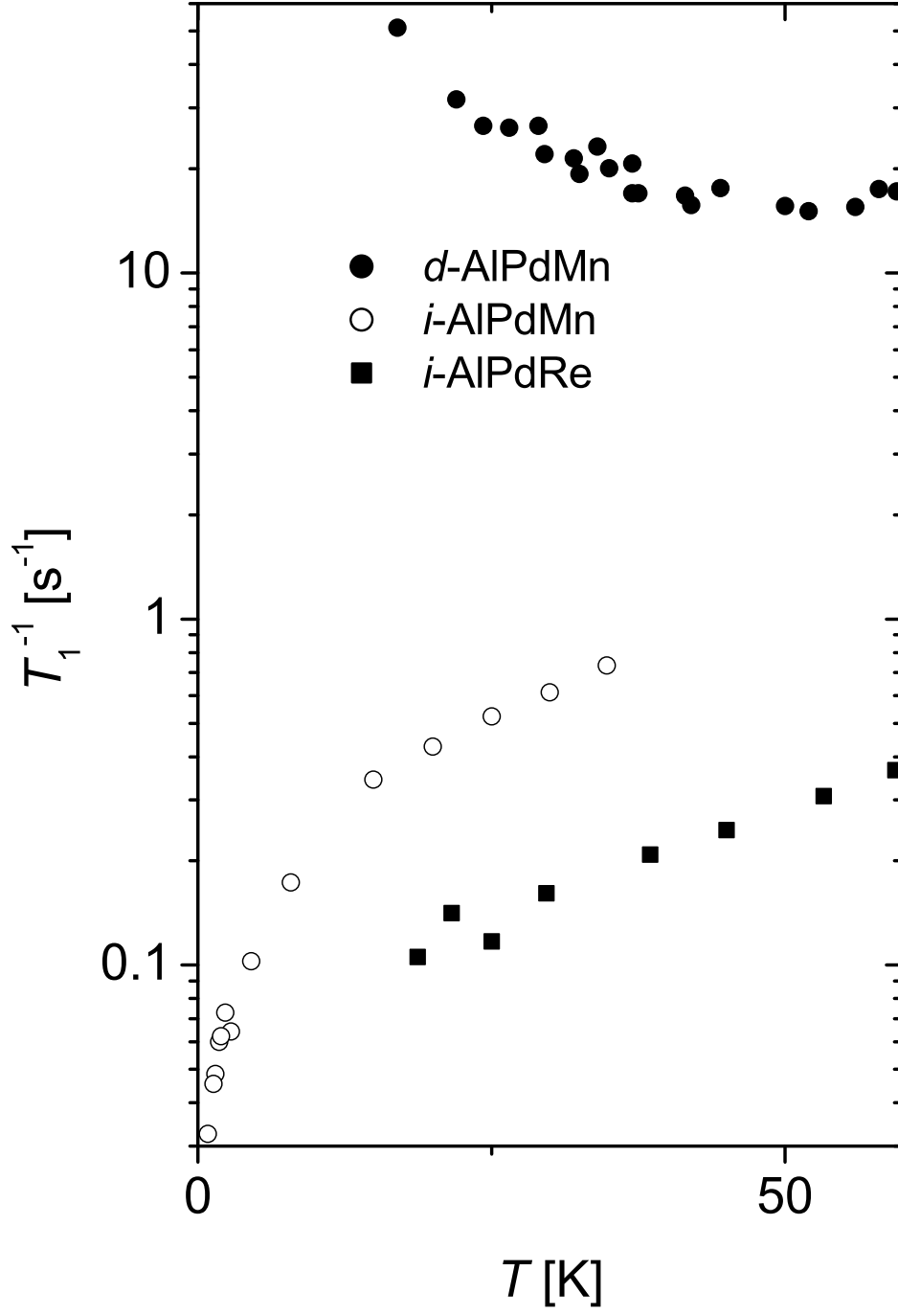


FIG. 12: Spin-lattice relaxation rates T_1^{-1} of ^{27}Al in the non-magnetic icosahedral quasicrystal i -AlPdRe[28], in icosahedral i -Al-Pd-Mn[14], and in d -Al-Pd-Mn.